Inhibition of quorum sensing in a computational biofilm simulation

J.A. Fozard[b,1,*], M. Lees[b,2], J.R. King[a], B.S. Logan[b]

[a] *School of Mathematical Sciences, University of Nottingham, Nottingham, United Kingdom.*
[b] *School of Computer Science, University of Nottingham, Nottingham, United Kingdom.*

Abstract

Bacteria communicate through small diffusible molecules in a process known as quorum sensing. Quorum-sensing inhibitors are compounds which interfere with this, providing a potential treatment for infections associated with bacterial biofilms. We present an individual-based computational model for a developing biofilm. Cells are aggregated into particles for computational efficiency, but the quorum-sensing mechanism is modelled as a stochastic process on the level of individual cells.

Simulations are used to investigate different treatment regimens. The response to the addition of inhibitor is found to depend significantly on the form of the positive feedback in the quorum-sensing model; in cases where the model exhibits bistability, the time at which treatment is initiated proves

*Corresponding author
Email addresses: john.fozard@nottingham.ac.uk (J.A. Fozard), mhlees@ntu.edu.sg (M. Lees), john.king@nottingham.ac.uk (J.R. King), bsl@cs.nott.ac.uk (B.S. Logan)
[1]Present address: Centre for Plant Integrative Biology, School of Biosciences, University of Nottingham, Sutton Bonnington Campus, Loughborough, United Kingdom.
[2]Present address: Division of Computer Science, Nanyang Technological University, Singapore.

to be critical for the effective prevention of quorum sensing and hence potentially of virulence.

Keywords: Bacteria, simulation, quorum sensing, inhibitor

1. Introduction

Under certain environmental conditions, planktonic bacteria (suspended in fluid) form multicellular structures known as biofilms on solid surfaces or at air-fluid interfaces. At a solid surface, bacteria first attach as single cells before forming microcolonies through clonal expansion, and further development of the biofilm includes movement across the surface and recruitment of more bacteria from the fluid phase (Stoodley et al., 2002). On attachment to the surface, bacteria often increase their rate of production of extracellular polymeric substances (EPS), generating a slimy coat (Branda et al., 2005). The microcolonies increase in size and coalesce, forming macrocolonies (Monds and O'Toole, 2009). Mature biofilms often have a complicated three-dimensional architecture with channels, pores and mushroom-like structures (O'Toole et al., 2000; de Kievit, 2009). Biofilms occur in many situations (see for example the review article of Costerton et al. (1987)). In a clinical context, biofilms are problematic through causing chronic and persistent infections on implants or damaged tissue. One bacterium of particular clinical significance is *Pseudomonas aeruginosa*, which causes infections in immunocompromised patients and chronic infections in the lungs of patients with cystic fibrosis (Moreau-Marquis et al., 2008).

Biofilms involve large numbers of bacteria in (multispecies) communities, and communication is important in coordinating the behaviour of multiple

cells (Waters and Bassler, 2005; Bassler and Losick, 2006). Many kinds of bacteria communicate through quorum-sensing molecules (QSMs), which they release into their local environment. (Williams and Cámara (2009) note that quorum sensing has been adopted as a generic term for bacterial signalling involving diffusible signalling molecules.) Depending on the species of bacteria in question, one of a number of QS mechanisms may be present (see the reviews Waters and Bassler (2005), Jayaraman and Wood (2008), and Ng and Bassler (2009)) and there may be multiple interacting circuits (e.g. in *P. aeruginosa* (Williams and Cámara, 2009)).

In Gram-negative bacteria, such as *P. aeruginosa*, acylated homoserine lactone (AHL) molecules are well-studied QSMs (Whitehead et al., 2001). These diffuse through bacterial membranes (Kaplan and Greenberg, 1985) and form a complex with LuxR-type transcriptional activator proteins (in some cases the AHLs are required for proper folding of the LuxR-type proteins (Zhu and Winans, 2001)). The resulting complex binds to the promoter regions of certain genes in the bacteria, greatly increasing their expression and that of associated downstream genes (e.g. Stevens et al. (1994)). One of these genes encodes the enzyme catalyzing production of QSM, so the QSM functions as an 'autoinducer', with the bacteria amplifying local levels of QSM (e.g. Seed et al. (1995)). This positive feedback loop causes bacteria to switch from a basal state of low QSM production to a state of high QSM production when the local concentration of QSM reaches a critical level. Local accumulation of QSM occurs if the cell density becomes (locally) high, or if transport of QSM away from the bacteria is inhibited (e.g. through being enclosed) (Hense et al., 2007; Platt and Fuqua, 2010). In this paper, cells in

states of high and low QSM production will be described as being up- and down-regulated, respectively.

Group behaviour mediated by quorum sensing occurs, for example, in luminescence in *Aliivibrio fisheri*, which is costly for an individual bacterium (in the open ocean), but beneficial at high cell densities within the light organs of certain squid (Waters and Bassler, 2005). It is also thought to influence biofilm development in several species of bacteria (Parsek and Greenberg, 2005), and to regulate swarming (Eberl et al., 1996; Kohler et al., 2000; Lindum et al., 1998; Daniels et al., 2004). In a wide range of bacteria, virulence gene expression is controlled by quorum sensing (Rumbaugh et al., 1999; Antunes et al., 2010). For *P. aeruginosa*, whilst the experimental evidence is conflicting (Parsek and Greenberg, 2005), biofilm structure has been seen to be affected by quorum sensing (Davies et al., 1998; Hentzer et al., 2002; Wang et al., 2007). It has been hypothesised that EPS production in *P. aeruginosa* is controlled by quorum sensing (Stoodley et al., 2002), with some authors reporting a difference in the structure of EPS produced by mutant strains which are defective in quorum sensing (Sauer et al., 2002); for a recent review see de Kievit (2009). EPS production is costly for individual bacteria, but may protect the biofilm as a whole and lead to an increased resistance to toxic compounds. EPS-producing strains of bacteria may also have an competitive advantage within a biofilm (Nadell et al., 2008).

Many types of bacteria have developed significant resistance to antibiotics. Bacteria in biofilms evade host defences, and these infections respond particularly poorly to conventional antimicrobial chemotherapy (Stewart and Costerton, 2001). One alternative approach to controlling bacterial infections

is to interfere with their quorum-sensing mechanisms (Williams, 2002). A number of compounds, such as the halogenated furanone compounds secreted by the macro-algae (seaweed) *Delisea pulchra* (Mansfield et al., 1999), or enzymes secreted by other bacteria (such as *Bacillus* species (Lee et al., 2002; Dong et al., 2002)), have been observed to inhibit quorum sensing through AHLs in *P. aeruginosa* (Reimmann et al., 2002; Hentzer et al., 2003). Halogenated furones bind to the transcriptional activator protein and enhance its degredation, whilst the bacterial enzymes act by degrading the QSM.

Their medical, environmental and industrial importance, as well as their intrinsic scientific interest, has led to extensive modelling studies of bacterial biofilms (see, e.g., the review of Klapper and Dockery (2010)), adopting a variety of continuum and individual- (or agent-) based approaches. Individual-based models (IBMs) are a common approach (e.g. Kreft et al., 1998, 2001; Chang et al., 2003; Picioreanu et al., 2004; Xavier et al., 2005a; Poplawski et al., 2008; Picioreanu et al., 2007), as it is relatively straightforward to integrate models for cellular level processes with continuum models for the diffusion of nutrients and signalling molecules within such a setting. Moreover, heterogeneity in the species and phenotype of the bacteria can be included more readily than in continuum models.

In the current paper we summarise a fairly generic IBM, which was developed to explore quorum-sensing processes and their inhibition, whilst being amenable to distributed computing. Quorum sensing was included in an IBM by Nadell et al. (2008), the latter work concentrating on competition between strains exhibiting and not exhibiting quorum sensing, and used a relatively simple model. Melke et al. (2010) recently included a model of the

underlying molecular mechanism for the Lux operon circuit within an IBM. The treatment of biofilms with quorum sensing inhibitors has been examined with continuum models by Anguige et al. (2004) and Frederick et al. (2011), but to our knowledge has not been considered in an individual-based setting by other workers. This paper extends upon Lees et al. (2007b) by having a simplified model for biomass shoving, a modified quorum sensing model (which includes positive feedback in the QSM production rate), and a different scheme to treat nutrient diffusion and uptake. We also make a more detailed investigation of the effects of QSI treatment on a developing biofilm. Unlike those in Nadell et al. (2008) and Melke et al. (2010), the quorum sensing model presented here includes stochastic effects which may be of particular significance to the autoinductive process of quorum sensing. This quorum sensing model is based on earlier deterministic models (Ward et al., 2001; Anguige et al., 2004).

In keeping with the above goals, we summarise the objectives of the paper as follows: we seek to explore the effectiveness of quorum sensing inhibitors in terms of their dependence on the properties of the quorum sensing network (monostable and bistable), the population size and the time of and level of exposure to inhibitors, with the intention of providing insight into what treatment protocols may be most effective. In particular, we explore the hypothesis that early treatment, before the population has achieved quorum, may be particularly beneficial. A subsidary aim of this study is to serve as a test case for the integration of cell-level models in the individual-based modelling approach. In particular, we will include increased EPS production by up-regulated cells as an example of the kinds of interactions between

quorum sensing and physical processes that may be investigated in such a framework.

2. Model

2.1. Representation of biofilm state

The model system represents a 3D 'biofilm reactor', with two compartments, bulk liquid and biofilm (see Figure 1). This is similar to that described in Picioreanu et al. (2004); differences include the incorporation here of (i) EPS production (note that EPS production is included in Xavier et al. (2005a), Kreft et al. (2001) and Lardon et al. (2011)) (ii) a quorum-sensing model, which requires particles to keep track of the number and states of the cells that they contain, and (iii) the use of a simpler voxel-based shoving model for biomass spreading. Here we incorporate only a single type of cell (and do not include 'inert' biomass generated by cell death) consuming a single substrate.

The bulk liquid compartment represents the environment away from the biofilm, and is well mixed, containing three diffusible substances, namely a soluble substrate (at concentration $c_{s,\mathrm{bulk}}$), which is consumed by the bacteria (Section 2.2.2), QSM (at concentration $c_{q,\mathrm{bulk}}$) and a diffusible quorum-sensing inhibitor (QSI), whose level, $c_{\bar{q},\mathrm{bulk}}$, we shall vary (Section 2.2.6); for simplicity, we assume that the concentration of QSM in the bulk liquid compartment is always zero ($c_{q,\mathrm{bulk}} = 0$). The top of the biofilm compartment is in contact with the bulk liquid compartment, and the two compartments exchange solutes solely by diffusion; this supplies suitable model boundary conditions upon the concentrations at the top of the biofilm compartment.

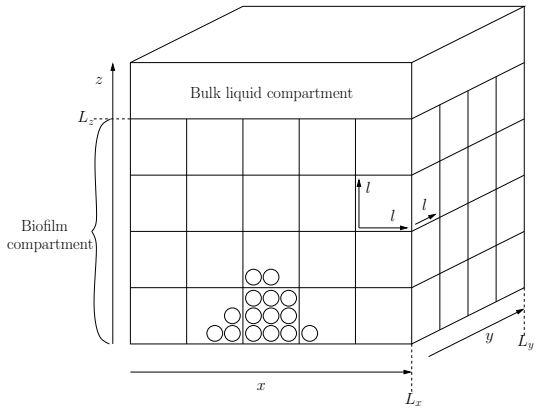

Figure 1: Schematic of the computational domain

The biofilm compartment is a rectangular cuboid, with periodic boundaries in the x- and y-directions, and a planar support at the base upon which the biofilm forms. In addition to substrate, QSM and QSI, the biofilm compartment contains biomass and EPS (Sections 2.1.1, 2.1.2). This compartment is further divided into voxels as discussed below (Section 2.1.2).

2.1.1. Particles

For efficiency of computation, individual cells are aggregated into biomass *particles*, as in Picioreanu et al. (2004). The cells contained within a particle consume substrate and grow (as described in Section 2.2.2). This causes the (dry) mass, M_j, of a particle to increase until it reaches a maximum mass, $M_{\max}$, at which point it divides, creating an additional particle (Section 2.2.4).

The number of cells within each particle varies with its mass: for simplicity, we take each particle to contain $n_j = \text{ceil}(M_j/M_{\text{ave}})$ cells, where M_{ave} is a typical mass of a cell and $\text{ceil}(x)$ denotes the smallest integer larger than or

equal to x. Each cell is in one of two states – up-regulated or down-regulated – between which it can instantaneously switch. Particles keep track of the numbers of up-regulated cells, u_j, and of down-regulated cells, d_j, that they contain, and these change in response to the local levels of QSM and QSI (see Section 2.2.6).

Cells produce EPS (Section 2.2.3), with the case in which up-regulated cells produce EPS at a much greater rate than down-regulated ones being of particular interest. Each voxel, e, keeps a record of the amount of EPS, E_e, that has been produced within it but has not been aggregated into EPS particles. When E_e exceeds a threshold value, M_{EPS}, the EPS is aggregated into an EPS particle; these do not grow, divide, consume substrate or participate in quorum sensing, but do occupy space in the voxels and can be displaced along with the biomass particles.

2.1.2. Voxels

The biofilm compartment is divided into (cubic) sub-compartments (*voxels*) containing particles, substrate and signalling molecules. The dimensions of the computational domain (L_x, L_y, L_z) are integer multiples of the voxel size, l. The voxels are fairly large in relation to the size of a cell, e.g., each voxel may contain of the order of 10^2 particles, typically corresponding to 10^4 cells.

Each voxel contains zero or more particles, and these exert a proliferative 'pressure' on those in the (six) adjacent voxels, this pressure being a function of the number of particles in the voxel. If there is a difference in pressure between neighbouring voxels, due to particle division for example, then particles may be displaced between them (see Section 2.2.5). This provides a

simple mechanism by which to redistribute particles in a way that reflects the limited space within a voxel. Each particle has a notional 3D position within its containing voxel, chosen at random (but avoiding overlap) that is used solely for visualisation purposes (see Figure 3).

As noted above, each voxel e keeps a record of the amount of EPS, E_e, that has been produced within it and has not yet been aggregated into particles. The voxels are also used to discretize the concentrations of soluble substances, which are approximated as uniform within in each voxel. The concentrations of substrate, QSM and QSI in voxel e are denoted by $c_{s,e}$, $c_{q,e}$ and $c_{\bar{q},e}$, respectively. The particles consume substrate and produce QSM (see Sections 2.2.2 and 2.2.6) and, along with diffusion, these processes change the concentrations in each voxel (Section 2.2.1).

2.2. Time evolution of model

We now describe how the state of the system changes during the simulations; for each of the components of the model, we explain how the state at $t = (T + 1)\Delta t$ is obtained from that at $t = T\Delta t$, where Δt is the global model timestep and T is an integer index. Much of this follows Picioreanu et al. (2004). Our model for diffusible substances is similar to theirs, but we adopt a fully time-dependent approach (rather than a quasi-steady one) in order to capture the quorum-sensing processes. The growth and division of biomass particles are dealt with as in Picioreanu et al. (2004), but with simpler (Monod) uptake rates and additional rules for changes in the numbers of up- and down-regulated cells. The model for biofilm expansion is somewhat simpler than that used in Picioreanu et al. (2004), as we do not consider the positions and radii of particles, but instead displace particles between voxels

depending upon the numbers of particles in the voxels and their neighbours (see Section 2.2.5). The model for quorum sensing that we adopt here is motivated by those of Ward et al. (2001) and Anguige et al. (2004). Various elements of the evolution of the system are stochastic: (as in Kreft et al. (1998)) the sizes of the daughter particles at division are chosen randomly in order to avoid synchronised division (see Section 2.2.4), the rule for particle shoving involves a random component to deal with the displacement of small numbers of particles (see Section 2.2.5) and the cells up- and down-regulate stochastically in order to represent quorum sensing with only two discrete states for each cell (see Section 2.2.6).

2.2.1. Diffusible substances

We evolve the voxel concentrations of substrate, QSM and QSI in time using a cell-centred finite-volume approximation. This leads to the semi-discrete equations

$$\frac{\mathrm{d}c_{\xi,e}}{\mathrm{d}t} = \frac{D_\xi}{l^2}\sum_{e'}(c_{\xi,e'} - c_{\xi,e}) + \frac{f_{\xi,e}}{l^3} \tag{1}$$

for each voxel e, where the sum is over all neighbours e' of e, ξ is one of $\{s, q, \bar{q}\}$, D_ξ is the appropriate diffusion coefficient and $f_{\xi,e}$ is the total net production rate within the voxel. We assume that the volume fraction occupied by cells or EPS has a negligible influence on the diffusion coefficients. (In the simulations, we shall take the diffusion coefficients for QSM and QSI to be equal.) As noted earlier, we take the domain to be periodic in the x- and y-directions. The planar support at the base of the biofilm compartment is impenetrable, i.e. the fluxes through it (corresponding to concentration

differences in (1)) are zero. The boundary conditions at the top of the biofilm compartment are implemented as a hypothetical layer of (ghost) voxels immediately above the biofilm compartment, each with the same concentrations as the bulk liquid compartment. Picioreanu et al. (2000) noted that, as the growth of particles occurs on a timescale which is much longer than that on which the substrate concentration relaxes to its equilibrium value across the whole domain, the substrate concentration may be considered to be at a quasi-steady state. While this steady-state elliptic problem can be solved very efficiently using iterative methods, simulation of quorum sensing requires a fully time-dependent approach with a sufficiently small time-step to resolve the up-regulation of cells.

Our emphasis here is in developing a flexible code in which additional effects can readily be incorporated. Whilst a fully implicit scheme might be computationally more efficient, we chose to treat the diffusion of all substances explicitly but the uptake of substrate implicitly. The time-step for such a scheme is limited by stability considerations, but to avoid this restricting the global time-step Δt, we evolve the concentrations over Δt using multiple sub-steps. For the QSM and QSI, we use S_q sub-steps of the forward Euler method with length $\Delta t/S_q < l^2/6D_q$, where this upper bound on the sub-step length is necessary for stability of the scheme and positivity of the solution. At each sub-step, we have

$$c_{q,e}^{T,\tau+1} = c_{q,e}^{T,\tau} + \frac{\Delta t}{S_q}\left(\frac{D_q}{l^2}\sum_{e'}\left(c_{q,e'}^{T,\tau} - c_{q,e}^{T,\tau}\right) + \frac{f_{q,e}^{T,0}}{l^3}\right) \tag{2}$$

(for the QSM, indicated by the subscript q), where the superscripts T, τ and

$T, \tau + 1$ here indicate the values at $t = T\Delta t + \tau\Delta t/S_q$ and $t = T\Delta t + (\tau + 1)\Delta t/S_q$, respectively. (Note that $\tau = 0$ and $\tau = S_q$ correspond to the start, $t = T\Delta t$, and end, $t = (T + 1)\Delta t$, of the global time-step.) The QSM production rate, $f_{q,e}^{T,0}$, is calculated at the start of each global time-step by aggregating the production rates for all particles contained in the voxel:

$$f_{q,e}^{T,0} = \sum_{j \in A(e)} w_j^{T,0} \tag{3}$$

where $A(e)$ is the set of indices of the particles contained in voxel e and the production rates w_j are given by (16) below. We treat the QSI identically, except that there is no production or consumption ($f_{\bar{q},e}^{T,0} = 0$).

If we were to use the same scheme for the substrate concentration, there would be an additional constraint upon the sub-step length because of the rapid rate at which a full voxel consumes substrate. We instead use S_s sub-steps of a simple first-order IMEX scheme (Ascher et al., 1995), where diffusion is treated explicitly and the uptake terms are treated by a linearly implicit method. This results in

$$c_{s,e}^{T,\tau+1} = c_{s,e}^{T,\tau} + \frac{1}{(1 - \Delta t J_{s,e}^{T,*}/S_s)} \frac{\Delta t}{S_s} \left(\frac{D_s}{l^2} \sum_{e'} \left(c_{s,e'}^{T,\tau} - c_{s,e}^{T,\tau} \right) + \frac{f_{s,e}^{T,*}}{l^3} \right), \tag{4}$$

where $f_{s,e}^{T,*}$ is the total net substrate production rate (minus the consumption rate) for all particles in voxel e, and $J_{s,e}^{T,*} = \partial f_{s,e}^{T,*}/\partial c_{s,e}$ is the derivative of $f_{s,e}^{T,*}$ with respect to the substrate concentration, calculated using

$$f_{s,e}^{T,*} = -\sum_{j \in A(e)} v_j^{T,*}, \qquad J_{s,e}^{T,*} = -\sum_{j \in A(e)} \frac{\partial v_j^{T,*}}{\partial c_{s,e}^{T,*}}, \tag{5}$$

where the particle substrate consumption rates, $v_j^{T,*}$, are given by (6). The asterisk denotes that these quantities are initially calculated at the start of each global time-step, but may be recalculated between sub-steps if necessary. We observed that the scheme became unstable (with the substrate concentration becoming negative) if the concentration changed significantly during a time-step. Therefore, we recalculate $f_{s,e}^{T,*}$ between sub-steps (using the updated voxel substrate concentrations) if the concentration in any voxel e changes by more than a prescribed amount (a relative change of 1%), which is found reliably to avoid the instability.

2.2.2. Growth of particles

The model for cell growth implemented in this simulation takes account of three separate processes: the uptake of substrate by the cells, the substrate required by the cells for maintenance, and the generation of new biomass (i.e. growth of the cells).

The cells contained in each particle consume substrate; we assume that the total consumption rate is proportional to the mass of the particle and depends upon the substrate concentration in the voxel containing the particle. For definiteness, following Kreft et al. (1998) we use Monod kinetics (Monod, 1949), for which the substrate uptake rate, v_j, is

$$v_j = V_{\max} \frac{c_{s,e}}{K_s + c_{s,e}} M_j, \tag{6}$$

where K_s is the half-saturation constant, and $V_{\max}$ is the maximum substrate uptake rate. Cells consume substrate for functions other than cell growth, and these maintenance requirements are taken to be proportional to the mass

of the cell. We model the mass of particles as increasing at a rate which is proportional to the excess substrate consumed, so

$$\frac{\mathrm{d}M_j}{\mathrm{d}t} = Y_{\max}(v_j - mM_j), \tag{7}$$

where m is the apparent maintenance rate of the cells (per unit mass, and in terms of the substrate consumed) at zero growth rate, whilst $Y_{\max}$ is the yield (efficiency at which substrate is converted into biomass). If the substrate uptake rate is insufficient to satisfy the maintenance requirements of the cells, then the particles shrink until uptake and maintenance balance. We evolve (7) in time using the forward Euler method, so

$$M_j^{T+1} = M_j^T + \Delta t Y_{\max}(v_j^T - mM_j^T), \tag{8}$$

where M_j^T denotes the mass of the particle with index j at $t = T\Delta t$.

Cell division is not considered explicitly, but the number of cells associated with a particle changes if its mass, M_j, passes through a multiple of the average cell mass, M_{ave}. For a growing particle the new cells are taken to be down-regulated (i.e. we increase the number of down-regulated cells, d_j.) Similarly, for a shrinking particle we, for definiteness, preferentially eliminate down-regulated rather than up-regulated cells. (If d_j is positive, we decrease d_j, but otherwise we decrease u_j.)

2.2.3. EPS production

Bacteria within a biofilm produce EPS, and in the model up- and down-regulated cells do so at constant rates $Z_{E,u}$ and $Z_{E,d}$, respectively. We are

particularly interested in the case where bacteria generate EPS at a greatly increased rate when up-regulated, which corresponds to $Z_{E,d} \ll Z_{E,u}$.

As discussed earlier, each voxel e records the amount of EPS, E_e, that has been generated within it but has not yet been aggregated into EPS particles. For each global time-step, we have

$$E_e^{T+1} = E_e^T + \Delta t \sum_{j \in A(e)} (Z_{E,d} d_j^T + Z_{E,u} u_j^T). \tag{9}$$

When E_e exceeds a threshold value, which we take to be $M_{\mathrm{EPS}} = (\rho_{\mathrm{EPS}}/\rho_c) M_{\max}$ (where ρ_c and ρ_{EPS} are the densities of cells and EPS in terms of their dry mass) so that an EPS particle corresponds to the same volume as a biomass particle immediately before division, we generate a new EPS particle in the voxel e. This new EPS particle has mass M_{EPS}, and we decrease E_e by M_{EPS}. Once created, EPS particles do not change mass.

2.2.4. Particle division

When the mass of a biomass particle exceeds the user-specified maximum, $M_{\max}$, it is split and a new daughter particle is created in the same voxel as the original particle. The mass of the daughter particle is chosen randomly from a uniform distribution with range between 0.4 and 0.6 of the mass of the particle at division, with the original particle retaining the remainder of the mass (i.e. the subdivision is approximately symmetric). The total number of up-regulated cells in the two particles is taken to be the same as in the parent particle; the up-regulated cells are distributed randomly between the two particles, weighted by the number of cells that they contain. (As the number of cells in each particle is rounded upwards, the two particles may

contain one more cell in total than the parent particle before division.)

2.2.5. Displacement

As we are not currently identifying the positions of particles *within* voxels (except for visualisation purposes), spreading does not occur within a single voxel. However, particles may be displaced between voxels. We here consider a simple model for particle displacement, biofilm stresses and other mechanical considerations not being the focus of the current investigation.

Particles are transferred between voxels if the difference in 'pressure' between the voxels is large enough. The pressure in voxel e, p_e, is:

$$p_e = \frac{N_e}{N_{\max} - N_e}, \tag{10}$$

where N_e is the total number of particles (including EPS) in the voxel and $N_{\max}$ is the maximum number of particles in a voxel; the latter is $N_{\max} = \rho_c \phi_{\max} l^3 / M_{\max}$, where ρ_c is the cell density (in terms of their dry mass) and $\phi_{\max}$ is the maximum volume fraction that the cells may occupy. Particles cannot pass through the planar support at the base of the biofilm compartment. The pressure above the biofilm compartment is taken to be zero, so particles can transfer freely into the bulk liquid compartment (at which point they are eliminated from the system). The total number of particles to be transferred out of the voxel e is given by

$$\Delta N_e = \sum_{e', p_{e'} < p_e} \text{floor}\left(\mu (p_e - p_{e'})(N_e - N_{e'})\right) \tag{11}$$

where μ is a *transfer coefficient* which specifies how easy it is to displace

particles, and the sum runs over all voxels e' neighbouring e with $p_{e'} < p_e$. Full voxels are handled specially: if $N_e > N_{\max}$, the total number of particles to transfer out of the voxel is $\Delta N_e = \text{ceil}(N_e - N_{\max})$, and the pressure is taken to be $p_e = \text{floor}(N_{\max})/(N_{\max} - \text{floor}(N_{\max}))$. The continuum limit corresponding to (10)–(11) is a doubly nonlinear diffusion equation (degenerate at $\partial N/\partial x = 0$ and singular at $N = N_{\max}$) that can be placed within well-established more general frameworks, associated with Darcy flow in particular. Indeed, the specific functional form (11) is of no real significance: a number of variants would lead to similar results and (11) is convenient for our purposes.

For each voxel e, we randomly select ΔN_e particles to transfer out of the voxel: to avoid artifacts for small values of ΔN_e, the direction in which each particle is displaced is chosen at random, with the probability of transferring a particle to a particular neighbouring voxel $\tilde{e}$ being

$$P_{e\to\tilde{e}} = \begin{cases} \dfrac{p_e - p_{\tilde{e}}}{\sum_{e',p_{e'}<p_e}(p_e - p_{e'})} & p_{\tilde{e}} < p_e, \\ 0 & p_{\tilde{e}} \geq p_e. \end{cases} \tag{12}$$

2.2.6. Quorum sensing

Here we adopt a generic (rather than species-specific) description of quorum sensing; similarly, the inhibitor modelling does not seek to account for specific mechanisms, but rather to illustrate the scope of the modelling approach described here. It is straightforward to include other effects, e.g. a substrate-dependent QSM production rate could be used to examine the interaction between the response to starvation and quorum sensing (Lazazzera,

2000).

We allow cells to switch randomly between up-regulated and down-regulated states at rates which depend upon the concentrations of QSM and QSI, $c_{q,e}$ and $c_{\bar{q},e}$, in the containing voxel, e. In the presence of inhibitor, the transition rate from down-regulated to up-regulated states is taken to be

$$Q^+ = \alpha \frac{c_{q,e}}{1 + \gamma(c_{q,e} + c_{\bar{q},e})}, \tag{13}$$

where α and γ are constants. In a small interval of length δt, the probability of a down-regulated cell becoming up-regulated is $Q^+(\delta t) + O((\delta t)^2)$, whilst the probability of a down-regulated cell remaining in that state is $1 - Q^+(\delta t) + O((\delta t)^2)$. The transition rate from up- to down-regulated states is taken to be

$$Q^- = \beta \frac{1 + \gamma c_{\bar{q},e}}{1 + \gamma(c_{q,e} + c_{\bar{q},e})}, \tag{14}$$

where β is the spontaneous down-regulation rate. The phenomenological equations (13)–(14) are chosen primarily on the basis that they represent the simplest appropriate saturating nonlinearities; that the same multiples of $c_{q,e}$ and $c_{\bar{q},e}$ appear in the denominators can be viewed as reflecting their relative scalings, while the appearance of γ in both numerator and denominator of (14) is a restrictive assumption, being a consequence of our policy of minimising the number of independent parameters.

Over one global time-step of length Δt, the numbers of up- and down-regulated cells evolve according to

$$u_j^{T+1} = u_j^T + X_1^T - X_2^T, \qquad d_j^{T+1} = n_j^T - u_j^{T+1}, \tag{15}$$

where X_1^n is a binomial random variable with d_j^T trials and success probability $Q^+\Delta t$, and X_2^n is a binomial random variable with u_j^T trials and success probability $Q^-\Delta t$. (As will be discussed in Section 2.2.7, we will apply (15) before the growth and division of particles; rules were given in Sections 2.2.2 and 2.2.4 for how these processes affect the numbers of up and down-regulated cells.) This scheme is similar to the binomial leap method of Tian and Burrage (2004), which is itself a variant of the explicit tau-leaping stochastic simulation algorithm (Gillespie, 2001).

The relevant bacteria generate QSM at a greatly increased rate when the QSM-activator complex is bound to the promoter region. To model this, we assume that up-regulated cells produce QSM at a rate $Z_{q,u}c_{q,e}/(K_q + c_{q,e})$, where K_q is a half-saturation constant, whilst down-regulated cells produce QSM at a constant rate $Z_{q,d} \ll Z_{q,u}$. The total production rate for each particle is therefore given by

$$w_j = Z_{q,u}\frac{c_{q,e}}{K_q + c_{q,e}}u_j + Z_{q,d}d_j. \tag{16}$$

We take the production rate to depend on the QSM concentration in order to explore the effects of different forms for the positive feedback in the QS mechanism – we do this in large part because the model exhibits bistability for $K_q \neq 0$ (see Figure 2). We also consider simulations in which the QSM production rate is independent of the local QSM concentration (following more closely the model of Ward et al. (2001)) by setting $K_q = 0$ in (16), in which case bistability does not occur (again see Figure 2). Thus the inclusion of K_q allows us to mimic the qualitative behaviour exhibited by more complex quorum-sensing models (notably bistability) without seeking to include more

specific gene circuitry.

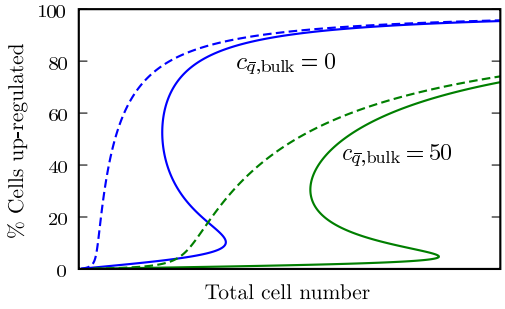

Figure 2: (colour online) Steady-state solutions of the (deterministic) quorum-sensing model for $K_q = 0$ (dashed lines) and $K_q = 10$ (solid lines), where K_q is the half-saturation constant in the QSM production rate function (16), and $c_{\bar{q},\mathrm{bulk}}$ is the QSI concentration in the bulk compartment. Assuming that the thickness of the biofilm is much smaller than L_z, the QSM concentration c_q is approximately uniform within the biofilm and a linear function of z above it. The percentages of up-regulated cells for which the expected net rate of up-regulation in the biofilm is zero are shown above. The system is bistable (in an intermediate range of cell number) for $K_q = 10$, thus exhibiting hysteresis, but monostable (albeit rapidly switching as the cell number is varied) for $K_q = 0$; in both cases, increasing the bulk inhibitor concentration $c_{\bar{q},\mathrm{bulk}}$ decreases the proportion of up-regulated cells.

2.2.7. Model time-step

In this section, we describe one time-step of the model, in order to define more precisely the order in which the computations are performed. At each time-step the voxels and particles are treated in two phases, with the diffusion calculation being performed between the two.

In the first phase for the voxels and particles, the QSM production rate, the growth rate and the substrate uptake rate (along with its derivative) are calculated for each particle using (16), (6) and (7). These are aggregated

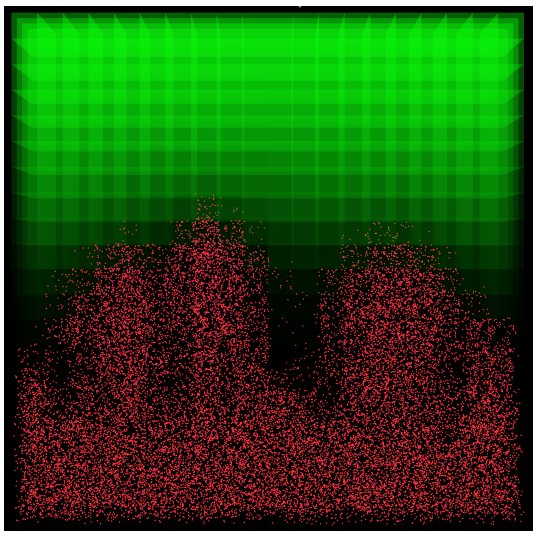

Figure 3: (colour online) Simulation visualisation. The green shading indicates the substrate concentration, whilst the red spheres are the biomass particles. The biofilm can be seen to be highly non-uniform, with fingering caused by competition for substrate between parts of the biofilm. Note that the domain size is different for these simulations ($L_x = L_z = 340$ μm, $L_y = 68$ μm) from that listed in Table 1 and used in the other simulations, and the bulk substrate concentration $c_{s,\mathrm{bulk}} = 0.1$. The domain is taken to be thin in the y direction in order to visualize the structure of the biofilm more clearly, whilst the height is taken to be smaller to promote non-uniform growth.

into totals for each voxel, and these totals are communicated to the diffusion module. The EPS production rate is also calculated for each particle, and the voxel EPS amounts E_e updated using (9); EPS particles are created in any voxel in which E_e exceeds the threshold M_{EPS}. In the course of this calculation, the numbers of up- and down-regulated cells within each biomass particle are updated using (15). The diffusion module then evolves the voxel concentrations using multiple sub-steps of (2) and (4). If the sub-

strate concentration in a voxel changes significantly during this calculation it is necessary to recompute the substrate uptake rate (and its derivative with respect to the substrate concentration) for that voxel. The voxel substrate, QSM and QSI concentrations are then updated.

In the second phase for the voxels and particles, the sizes of the biomass particles are updated (using (8) and the substrate uptake rates calculated in the first phase), and those particles that have exceeded the maximum mass are subdivided. The voxels then execute a displacement step. For each voxel, the pressure is calculated using (10), and the number of particles to be displaced out of the voxel is given by (11). These particles are selected at random and removed from the voxel, and the voxels into which these are displaced are chosen at random according to (12). The simulation time, t, is then incremented by Δt, and the cycle is repeated using the newly calculated voxel concentrations and particles.

2.3. Parameters and initial conditions

The parameter values for bacterial growth were taken from Kreft et al. (1998), and the parameters for the quorum-sensing were based on those in Koerber et al. (2002). We chose the voxel size to be $l = 17\mu m$, to give the same spatial resolution for the concentrations of soluble substances as in Picioreanu et al. (2004). The default parameter values are listed in Table 1. At the start of the simulations, the voxels in the bottom layer of the biofilm compartment were populated with 10 biomass particles each (approximately 20% of the maximum capacity, $N_{\max}$), and the initial masses, M_j, of these particles were chosen at random from a uniform distribution on $400 < M_j < 800$. All cells were initially down-regulated. In each voxel, the EPS amounts,

E_e, and the concentrations of QSM and QSI, $c_{q,e}$ and $c_{\bar{q},e}$, were taken to be zero initially, whilst the substrate concentrations, $c_{s,e}$, were taken to be the same as that in the bulk liquid compartment, $c_{s,\mathrm{bulk}}$.

3. Results and Discussion

We use our simulations to investigate quorum sensing in a developing biofilm and the treatment of such a biofilm with a QSI. Figure 3 illustrates the types of complex behaviour that the model can exhibit; it is not, however, our goal here to investigate such morphologies (which have been the subject of detailed studies in their own right e.g. by Dockery and Klapper (2001)).

In the first set of computational experiments, we examine the behaviour of a biofilm in the absence of QSI. We consider a range of values for the substrate concentration in the bulk liquid compartment ($c_{s,\mathrm{bulk}} = 0.1, 0.2, 0.3$) in order to produce biofilms that grow at different rates. Figure 4a shows the total number of cells and the number of up-regulated cells over the course of simulations in which the rate of QSM production by up-regulated cells depends on its local concentration ($K_q = 10$). The total number of cells initially increases exponentially, but this growth soon becomes linear owing to substrate limitations. Near the start of the simulations, most of the cells are down-regulated, but after several hours quorum sensing occurs, with the proportion of up-regulated cells increasing significantly over a period of about 1 hr; this event occurs at an earlier time for higher bulk substrate concentrations, as the number of cells in the biofilm increases more rapidly. Figure 4b shows simulations in which the QSM production rate by up-regulated cells is independent of the local QSM concentration ($K_q = 0$). With the other

Parameter	Value	Units	Source
L_x, L_y	170	μm	(Num)
L_z	1700	μm	(Num)
l	17	μm	(Num)
Δt	0.083	min	(Num)
$M_{\max}$	14700	fg	(Num)
M_{ave}	410	fg	(Est)
ρ_c	290	fg fl^{-1}	(Kr)
ρ_{EPS}	290	fg fl^{-1}	(Est)
$\phi_{\max}$	0.52	n/a	(Est)
$c_{s,\text{bulk}}$	0.2	fg fl^{-1}	(Est)
D_s	40680	μm^2 min^{-1}	(Kr)
D_q, $D_{\bar{q}}$	33300	μm^2 min^{-1}	(Ko)
S_q, $S_{\bar{q}}$	10	n/a	(Num)
S_s	12	n/a	(Num)
$V_{\max}$	0.046	min^{-1}	(Kr)
m	6×10^{-4}	min^{-1}	(Kr)
$Y_{\max}$	0.444	n/a	(Kr)
K_s	2.34×10^{-3}	fg fl^{-1}	(Kr)
$Z_{E,d}$	0	fg min^{-1}	(Est)
$Z_{E,u}$	0.001	fg min^{-1}	(Est)
μ	0.001	n/a	(Est)
$N_{\max}$	50.4	n/a	(Num)
α	1.33	fl min^{-1} molecule^{-1}	(Ko)
β	10	min^{-1}	(Ko)
γ	0.1	fl molecules^{-1}	(Est)
$Z_{q,u}$	8.3	molecules min^{-1}	(Ko)
$Z_{q,d}$	1230	molecules min^{-1}	(Ko)
K_q	10	molecules fl^{-1}	(Est)
t_0	$0^\dagger$	min	(Est)
$C_{\bar{q}}$	$0^\dagger$	molecules fl^{-1}	(Est)

Table 1: Default parameter set. (Kr) = Kreft et al. (1998), (Ko) = Koerber et al. (2002), (Num) = parameters for numerical approximation, (Est) = physical parameters estimated for this simulation. † QSI is not added in the default simulations.

parameters taking the same values, quorum sensing occurs earlier than in Figure 4a, largely because the QSM production rate (16) is now larger at small QSM concentrations.

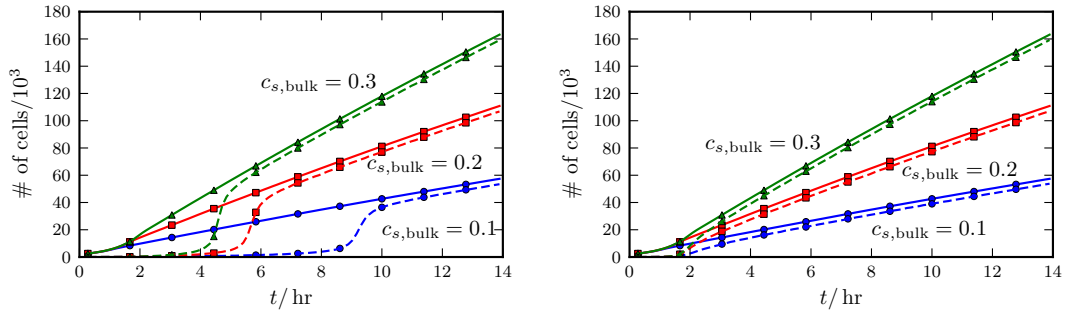

(a) $K_q = 10$ (b) $K_q = 0$

Figure 4: (colour online) Growth and quorum sensing in biofilms without QSI. Here K_q is the half-saturation constant in the QSM production rate function (16), and $c_{s,\text{bulk}}$ is the substrate concentration in the bulk compartment. The solid lines show the increase in the total numbers of cells over time, whilst the dashed lines are the numbers of up-regulated cells. $c_{s,\text{bulk}} = 0.1, 0.2, 0.3$ corresponds to blue with circular markers, red with square markers and green with triangular markers respectively. (For interpretation of the references to color in this caption, the reader is referred to the web version of the article.)

The second set of experiments investigate the effect of QSI upon a developing biofilm, with the substrate concentration in the bulk compartment fixed at $c_{s,\text{bulk}} = 0.2$. There is a delay, t_0, before the initial application of the QSI, and for $t > t_0$ the QSI concentration in the bulk compartment $c_{\bar{q},\text{bulk}}$ is held at a constant value $C_{\bar{q}}$. Simulations with $K_q = 10$ are shown in Figure 5a–(c). In the absence of QSI, quorum sensing occurs roughly 6 hours after the start of the simulations. With low levels of QSI ($C_{\bar{q}} = 50$, Figure 5a), the

number of up-regulated cells is only slightly diminished if the QSI is added during or after the onset of quorum sensing ($t_0 = 6$ hr, 7 hr). However, if the QSI is introduced earlier ($t_0 = 5$ hr), the proportion of up-regulated cells stays much lower for several hours, before eventually increasing to the same level as when the QSI is added later. This is presumably a consequence of the bistability of the quorum-sensing mechanism; if the QSI is added earlier, the system is attracted to the state with a low proportion of up-regulated cells and remains there until the total cell number grows too large and bistability is lost (cf. Figure 2), whilst if the QSI is added later, the system is rapidly attracted to the state in which a higher proportion of the cells are up-regulated. Such behaviour has obvious therapeutic implications, particularly when quorum sensing is associated with virulence, such effects having been investigated in a deterministic continuum context by Anguige et al. (2004). Increasing the level of QSI ($C_{\bar{q}} = 100, 150$, Figures 5b, 5c) leads to a lower proportion of cells being up-regulated. If the biofilm is treated before the onset of quorum sensing ($t_0 = 5$ hr), increasing the applied QSI concentration, $C_{\bar{q}}$, also increases the period of time for which the proportion of up-regulated cells stays at a low level. At the highest levels of QSI considered here ($C_{\bar{q}} = 150$), the number of up-regulated cells drops to a low level even when the biofilm is treated midway through quorum sensing ($t_0 = 6$ hr).

Simulations with $K_q = 0$ are shown in Figure 5d–(f). As up-regulation now occurs after roughly 2 hr, we treat the biofilm with QSI earlier ($t_0 =$ 1 hr, 2 hr, 4 hr). In this case, the quorum-sensing mechanism has only one stable deterministic steady state (see Figure 2). Increasing the applied QSI concentration, $C_{\bar{q}}$, again decreases the proportion of up-regulated cells.

Whilst earlier application of the QSI (smaller t_0) again leads to the number of up-regulated cells being lower at later times, this effect is markedly less significant than with $K_q = 10$.

The EPS production rate in the above simulations is relatively small ($Z_{E,u} = 0.001$). To examine whether EPS production has any significant effect upon quorum sensing, simulations were performed with substantially higher EPS production rates ($Z_{E,u} = 50$). As before, the bulk substrate concentration is set at $c_{s,\mathrm{bulk}} = 0.2$ and the biofilm is treated with QSI, with $C_{\bar{q}} = 100$ and $t_0 = 10$ hr. The results of these simulations are shown in Figure 6, for both $K_q = 10$ and $K_q = 0$. The total cell number is slightly larger at the higher EPS production rate: EPS production reduces the density of cells, leading to a reduced substrate consumption per unit thickness, and higher substrate concentrations deep within the biofilm. (Increased EPS production also increases the thickness of the biofilm, and this reduces the distance that the substrate needs to diffuse from the bulk liquid compartment.)

GFP reporter constructs have been developed which allow measurement of QSM levels and the intensity of the quorum sensing response within a biofilm (Hentzer et al., 2003; Duan and Surette, 2007). These data show a rapid increase in transcription of genes under the control of a number of different promoters associated with the *las* quorum sensing mechanism several hours after the start of the experiment. These reporter systems have also been used to examine the effects of various QSIs upon a developing biofilm; treatment diminishes the maximim amplitude of the response, and appears to slightly delay its onset (Rasmussen et al., 2005a,b). However, in these experiments the QSI is added at the start (held at a constant level),

rather than being added midway through the quorum sensing response (as in our computational simulations here). One significant difference between the experimental measurements and the results of our model is that in the experiments the expression of components of the quorum sensing system appear to attain a maximum and then decline, whilst this does not occur in the simulations. The mechanism is for this is unclear, but it would be instructive to include more detail of the quorum sensing response, in particular negative feedback through the QSM-stimulated production of a QS repressor protein such as RsaL (de Kievit et al., 1999).

Our simulations suggest that the timing of application of the QSI is important for the successful prevention of quorum sensing; if the QSI is added before the time at which most of the colony up-regulates, then the bulk of the cells remain down-regulated for a significant length of time, whilst if the same concentration of QSI is added later, there is only a relatively small decrease in the proportion of up-regulated cells. This difference is most pronounced in the case where the QSM production rate depends on the local QSM concentration ($K_q > 0$). In practical treatments, it is likely that the QSI will be applied periodically (Hentzer et al., 2003), and so the bulk concentration of QSI will vary with time. If the quorum-sensing system exhibits bistability, then it is important that the QSI levels remain sufficiently high throughout the treatment. The simulations of this paper indicate that it would be interesting to perform experiments in which the biofilm is treated with QSI midway through the quorum sensing response; this would test whether such treatments are likely to be effective if applied after the initial formation of microcolonies, and also provide a way of investigating the bistability of the

underlying QS system. The combination of QSI with conventional antibiotics is also likely to be of interest (Rasmussen et al., 2005a,b), and mathematical modelling may be of great use in helping develop appropriate treatment regimes.

The model for quorum sensing considered here is more complex than that of Nadell et al. (2008), but significantly simpler than that of Melke et al. (2010). In particular, the model captures stochastic effects, which may be important for the timing of the onset of quorum sensing, with a minimal amount of computational effort; simulating a stochastic system of reactions (using e.g. the Gillespie stochastic simulation algorithm (Gillespie, 1977)) within each bacteria would be much more computationally expensive. The model is also more suited than that of Melke et al. (2010) to simulations in which groups of bacteria are aggregated into particles for computational efficiency (following Picioreanu et al. (2004) and Xavier et al. (2005a), for example).

Many of the elements of this model could be made more sophisticated. The model for biomass spreading and EPS could include more physical effects (cf. Alpkvist et al., 2006). It would also be instructive to include models for biofilm detachment (Xavier et al., 2005b), as this may be important in the effect of QSIs on biofilm structure and in their susceptibility to surfactants (Hentzer et al., 2003). We have also neglected much of the complexity of the different substrates consumed and produced by bacteria (e.g. oxygen) that has been included in other models (Kreft et al., 2001; Picioreanu et al., 2004; Xavier et al., 2005a; Lardon et al., 2011).

Although the simulations in this paper were performed on a single pro-

cessor, a preliminary version of the software used was adapted to allow distributed simulation of models on clusters and Grids (Logan et al., 2006; Lees et al., 2007a). It would be relatively straightforward to integrate the more sophisticated bacterial models described here into the distributed framework, and this would be of particular benefit for the future inclusion of more detailed cell-level processes: indeed, some of the design decisions made in the development of the simulator, in particular the rules used for particle motion and the scheme used for diffusible substances, were motivated by this possibility.

3.1. Conclusions

In summary, we have developed a three-dimensional, stochastic individual-based model for a developing biofilm which captures quorum sensing on the level of individual cells, illustrating (albeit in a greatly simplified framework) the scope for incorporating subcellular pathways into multiscale models of this type. This model was used to investigate the treatment of developing biofilms by quorum sensing inhibitors, and we found that the timing of the treatment was important. Whilst the processes involved are complex and the model used is simplistic in a number of regards, such approaches seem to have considerable promise in understanding the macroscopic (population-scale) manifestations of more and more complex genetic, signalling and metabolic networks.

ACKNOWLEDGEMENTS

This work was supported by BBSRC project number BB/D006619/1 and by EPSRC projects GR/S82862/01, EP/C549406/1 and EP/C549414/1.

JRK also gratefully acknowledges the support of the Royal Society and Wolfson Foundation.

References

Alpkvist, E., Picioreanu, C., van Loosdrecht, M.C., Heyden, A., 2006. Three-dimensional biofilm model with individual cells and continuum EPS matrix. Biotechnol. Bioeng. 94, 961–979.

Anguige, K., King, J.R., Ward, J.P., Williams, P., 2004. Mathematical modelling of therapies targeted at bacterial quorum sensing. Math. Biosci. 192, 39–83.

Antunes, L.C., Ferreira, R.B., Buckner, M.M., Finlay, B.B., 2010. Quorum sensing in bacterial virulence. Microbiology (Reading, Engl.) 156, 2271–2282.

Ascher, U.M., Ruuth, S.J., Wetton, B.T.R., 1995. Implicit-explicit methods for time-dependent partial differential equations. SIAM J. Numer. Anal. 32, 797–823.

Bassler, B.L., Losick, R., 2006. Bacterially speaking. Cell 125, 237–246.

Branda, S.S., Vik, S., Friedman, L., Kolter, R., 2005. Biofilms: the matrix revisited. Trends Microbiol. 13, 20–26.

Chang, I., Gilbert, E.S., Eliashberg, N., Keasling, J.D., 2003. A three-dimensional, stochastic simulation of biofilm growth and transport-related factors that affect structure. Microbiology 149, 2859–2871.

Costerton, J.W., Cheng, K.J., Geesey, G.G., Ladd, T.I., Nickel, J.C., Dasgupta, M., Marrie, T.J., 1987. Bacterial biofilms in nature and disease. Annu. Rev. Microbiol. 41, 435–464.

Daniels, R., Vanderleyden, J., Michiels, J., 2004. Quorum sensing and swarming migration in bacteria. FEMS Microbiol. Rev. 28, 261–289.

Davies, D.G., Parsek, M.R., Pearson, J.P., Iglewski, B.H., Costerton, J.W., Greenberg, E.P., 1998. The involvement of cell-to-cell signals in the development of a bacterial biofilm. Science 280, 295–298.

Dockery, J., Klapper, I., 2001. Finger formation in biofilm layers. SIAM J. Appl. Math. 62, 853–869.

Dong, Y.H., Gusti, A.R., Zhang, Q., Xu, J.L., Zhang, L.H., 2002. Identification of quorum-quenching n-acyl homoserine lactonases from *Bacillus* species. Appl. Environ. Microbiol. 68, 1754–1759.

Duan, K., Surette, M.G., 2007. Environmental regulation of *Pseudomonas aeruginosa* PAO1 Las and Rhl quorum-sensing systems. J. Bacteriol. 189, 4827–4836.

Eberl, L., Winson, M.K., Sternberg, C., Stewart, G.S., Christiansen, G., Chhabra, S.R., Bycroft, B., Williams, P., Molin, S., Givskov, M., 1996. Involvement of N-acyl-L-hormoserine lactone autoinducers in controlling the multicellular behaviour of Serratia liquefaciens. Mol. Microbiol. 20, 127–136.

Frederick, M.R., Kuttler, C., Hense, B.A., Eberl, H.J., 2011. A mathematical

model of quorum sensing regulated EPS production in biofilm communities. Theor Biol Med Model 8, 8.

Gillespie, D.T., 1977. Exact stochastic simulation of coupled chemical reactions. J. Phys. Chem. 81, 2340–2361.

Gillespie, D.T., 2001. Approximate accelerated stochastic simulation of chemically reacting systems. J. Chem. Phys. 115, 1716.

Hense, B.A., Kuttler, C., Muller, J., Rothballer, M., Hartmann, A., Kreft, J.U., 2007. Does efficiency sensing unify diffusion and quorum sensing? Nat. Rev. Microbiol. 5, 230–239.

Hentzer, M., Riedel, K., Rasmussen, T.B., Heydorn, A., Andersen, J.B., Parsek, M.R., Rice, S.A., Eberl, L., Molin, S., Høiby, N., Kjelleberg, S., Givskov, M., 2002. Inhibition of quorum sensing in *Pseudomonas aeruginosa* biofilm bacteria by a halogenated furanone compound. Microbiology 148, 87–102.

Hentzer, M., Wu, H., Andersen, J.B., Riedel, K., Rasmussen, T.B., Bagge, N., Kumar, N., Schembri, M.A., Song, Z., Kristoffersen, P., Manefield, M., Costerton, J.W., Molin, S., Eberl, L., Steinberg, P., Kjelleberg, S., Høiby, N., Givskov, M., 2003. Attenuation of *Pseudomonas aeruginosa* virulence by quorum sensing inhibitors. EMBO J. 22, 3803–3815.

Jayaraman, A., Wood, T.K., 2008. Bacterial quorum sensing: Signals, circuits, and implications for biofilms and disease. Ann. Rev. Biomed. Eng. 10, 145–167.

Kaplan, H.B., Greenberg, E.P., 1985. Diffusion of autoinducer is involved in regulation of the Vibrio fischeri luminescence system. J. Bacteriol. 163, 1210–1214.

de Kievit, T., Seed, P.C., Nezezon, J., Passador, L., Iglewski, B.H., 1999. RsaL, a novel repressor of virulence gene expression in Pseudomonas aeruginosa. J. Bacteriol. 181, 2175–2184.

de Kievit, T.R., 2009. Quorum sensing in Pseudomonas aeruginosa biofilms. Environ. Microbiol. 11, 279–288.

Klapper, I., Dockery, J., 2010. Mathematical description of microbial biofilms. SIAM Rev. 52, 221–265.

Koerber, A.J., King, J.R., Ward, J.P., Williams, P., Croft, J.M., Sockett, R.E., 2002. A mathematical model of partial-thickness burn-wound infection by *Pseudomonas aeruginosa*: Quorum sensing and the build-up to invasion. Bull. Math. Biol. 64, 239–259.

Kohler, T., Curty, L.K., Barja, F., van Delden, C., Pechere, J.C., 2000. Swarming of Pseudomonas aeruginosa is dependent on cell-to-cell signaling and requires flagella and pili. J. Bacteriol. 182, 5990–5996.

Kreft, J.U., Booth, G., Wimpenny, J.W.T., 1998. BacSim, a simulator for individual-based modelling of bacterial colony growth. Microbiology 144, 3275–3287.

Kreft, J.U., Picioreanu, C., Wimpenny, J.W., van Loosdrecht, M.C., 2001. Individual-based modelling of biofilms. Microbiology 147, 2897–2912.

Lardon, L.A., Merkey, B.V., Martins, S., Dotsch, A., Picioreanu, C., Kreft, J.U., Smets, B.F., 2011. iDynoMiCS: next-generation individual-based modelling of biofilms. Environ Microbiol .

Lazazzera, B.A., 2000. Quorum sensing and starvation: signals for entry into stationary phase. Curr. Opin. Microbiol. 3, 177–182.

Lee, S.J., Park, S.Y., Lee, J.J., Yum, D.Y., Koo, B.T., Lee, J.K., 2002. Genes encoding the n-acyl homoserine lactone-degrading enzyme are widespread in many subspecies of *Bacillus thuringiensis*. Appl. Environ. Microbiol. 68, 1754–1759.

Lees, M., Logan, B.S., King, J.R., 2007a. HLA simulation of agent-based bacterial models, in: Proceedings of the 2007 European Simulation Interoperability Workshop, Simulation Interoperability Standards Organisation, Genoa. 07E-SIW-032.

Lees, M., Logan, B.S., King, J.R., 2007b. Multiscale models of bacterial populations, in: Henderson, S.G., Biller, B., Hsieh, M.H., Shortle, J., Tew, J.D., Barton, R.R. (Eds.), Proceedings of the 2007 Winter Simulation Conference, IEEE Press. pp. 881–890.

Lindum, P.W., Anthoni, U., Christophersen, C., Eberl, L., Molin, S., Givskov, M., 1998. N-Acyl-L-homoserine lactone autoinducers control production of an extracellular lipopeptide biosurfactant required for swarming motility of Serratia liquefaciens MG1. J. Bacteriol. 180, 6384–6388.

Logan, B.S., Lees, M., King, J.R., 2006. Bacgrid: Large scale systems biology simulation on the grid, in: Winter Simulation Conference, Track on

Modelling and Simulation in Computational Biology, Monterey, CA USA. (poster).

Mansfield, M., de Nys, R., Kumar, N., Read, R., Givskov, M., Steinberg, P., Kjelleberg, S., 1999. Evidence that halogenated furanones from *Delisea pulchra* inhibit acylated homoserine lactone (AHL)-mediated gene expression by displacing the AHL signal from its receptor protein. Microbiology 145, 283–291.

Melke, P., Sahlin, P., Levchenko, A., Jonsson, H., 2010. A cell-based model for quorum sensing in heterogeneous bacterial colonies. PLoS Comput. Biol. 6, e1000819.

Monds, R.D., O'Toole, G.A., 2009. The developmental model of microbial biofilms: ten years of a paradigm up for review. Trends Microbiol. 17, 73–87.

Monod, J., 1949. The growth of bacterial cultures. Annu. Rev. Microbiol. 3, 371–394.

Moreau-Marquis, S., Stanton, B.A., O'Toole, G.A., 2008. *Pseudomonas aeruginosa* biofilm formation in the cystic fibrosis airway. Pulm. Pharmacol. Ther. 21, 595–599.

Nadell, C.D., Xiavier, J.B., Levin, S.A., Foster, K.R., 2008. The evolution of quorum sensing in bacterial biofilms. PLoS Biol. 16, 171–179.

Ng, W.L., Bassler, B.L., 2009. Bacterial quorum-sensing network architectures. Annu. Rev. Genet. 43, 197–222.

O'Toole, G., Kaplan, H.B., Kolter, R., 2000. Biofilm formation as microbial development. Annu. Rev. Microbiol. 54, 49–79.

Parsek, M.R., Greenberg, E.P., 2005. Sociomicrobology: the connections between quorum sensing and biofilms. Trends microbiol. 13, 29–33.

Picioreanu, C., Kreft, J.U., Klausen, M., Haagensen, J.A., Tolker-Nielsen, T., Molin, S., 2007. Microbial motility involvement in biofilm structure formation–a 3D modelling study. Water Sci. Technol. 55, 337–343.

Picioreanu, C., Kreft, J.U., van Loosdrecht, M.C.M., 2004. Particle-based multidimensional multispecies biofilm model. Appl. Environ. Microbiol. 70, 3024–3040.

Picioreanu, C., van Loosdrecht, M.C.M., Heijnen, J.J., 2000. Effect of diffusive and convective substrate transport on biofilm structure formation: a two-dimensional modelling study. Biotechnol. Bioeng. 69, 504–515.

Platt, T.G., Fuqua, C., 2010. What's in a name? The semantics of quorum sensing. Trends Microbiol. 18, 383–387.

Poplawski, N.J., Shirinifard, A., Swat, M., Glazier, J.A., 2008. Simulation of single-species bacterial-biofilm growth using the Glazier-Graner-Hogeweg model and the CompuCell3D modeling environment. Math. Biosci. Eng. 5, 355–388.

Rasmussen, T.B., Bjarnsholt, T., Skindersoe, M.E., Hentzer, M., Kristoffersen, P., Kote, M., Nielsen, J., Eberl, L., Givskov, M., 2005a. Screening for quorum-sensing inhibitors (QSI) by use of a novel genetic system, the QSI selector. J. Bacteriol. 187, 1799–1814.

Rasmussen, T.B., Skindersoe, M.E., Bjarnsholt, T., Phipps, R.K., Christensen, K.B., Jensen, P.O., Andersen, J.B., Koch, B., Larsen, T.O., Hentzer, M., Eberl, L., Hoiby, N., Givskov, M., 2005b. Identity and effects of quorum-sensing inhibitors produced by Penicillium species. Microbiology (Reading, Engl.) 151, 1325–1340.

Reimmann, C., Ginet, N., Michel, L., Keel, C., Michaux, P., Krishnapillai, V., Zala, M., Heurlier, K., Triandafillu, K., Harms, H., Défago, G., Haas, D., 2002. Genetically programmed autoinducer destruction reduces virulence gene expression and swarming motility in *Pseudomonas aeruginosa* PAO1. Microbiology 148, 923–932.

Rumbaugh, K.P., Griswold, J.A., Iglewski, B.H., Hamood, A.N., 1999. Contribution of quorum sensing to the virulence of Pseudomonas aeruginosa in burn wound infections. Infect. Immun. 67, 5854–5862.

Sauer, K., Camper, A.K., Ehrlich, G.D., Costerton, J.W., Davies, D.G., 2002. *Pseudomonas aeruginosa* displays multiple phenotypes during development as a biofilm. J. Bacteriol. 184, 1140–1154.

Seed, P.C., Passador, L., Iglewski, B.H., 1995. Activation of the Pseudomonas aeruginosa lasI gene by LasR and the Pseudomonas autoinducer PAI: an autoinduction regulatory hierarchy. J. Bacteriol. 177, 654–659.

Stevens, A.M., Dolan, K.M., Greenberg, E.P., 1994. Synergistic binding of the Vibrio fischeri LuxR transcriptional activator domain and RNA polymerase to the lux promoter region. Proc. Natl. Acad. Sci. U.S.A. 91, 12619–12623.

Stewart, P.S., Costerton, J.W., 2001. Antibiotic resistance of bacteria in biofilms. Lancet 14, 135–138.

Stoodley, P., Sauer, K., Davies, D.G., Costerton, J.W., 2002. Biofilms as complex differentiated communities. Annu. Rev. Microbiol. 56, 187–209.

Tian, T., Burrage, K., 2004. Binomial leap methods for simulating stochastic chemical kinetics. J. Chem. Phys. 121, 10356–10364.

Wang, Y., Dai, Y., Zhang, Y., Hu, Y., Yang, B., Chen, S., 2007. Effects of quorum sensing autoinducer degradation gene on virulence and biofilm formation of *Pseudomonas aeruginosa*. Sci. China, C, Life Sci. 50, 385–391.

Ward, J.P., King, J.R., Koerber, A.J., Williams, P., Croft, J.M., Sockett, R.E., 2001. Mathematical modelling of quorum sensing in bacteria. Math. Med. Biol. 18, 263–292.

Waters, C.M., Bassler, B.L., 2005. Quorum sensing: cell-to-cell communication in bacteria. Annu. Rev. Cell Dev. Biol. 21, 319–346.

Whitehead, N.A., Barnard, A.M., Slater, H., Simpson, N.J., Salmond, G.P., 2001. Quorum-sensing in Gram-negative bacteria. FEMS Microbiol. Rev. 25, 365–404.

Williams, P., 2002. Quorum sensing: an emerging target for antibacterial chemotherapy? Exp. Opin. Ther. Targets 6, 257–274.

Williams, P., Cámara, M., 2009. Quorum sensing and environmental adaptation in *Pseudomonas aeruginosa*: a tale of regulatory networks and multifunctional signal molecules. Curr. Opin. Microbiol. 12, 182–191.

Xavier, J.B., Picioreanu, C., van Loosdrecht, M.C.M., 2005a. A framework for multidimensional modelling of activity and structure of multispecies biofilms. Appl. Env. Microbiol. 7, 1085–1103.

Xavier, J.d.e.B., Picioreanu, C., van Loosdrecht, M.C., 2005b. A general description of detachment for multidimensional modelling of biofilms. Biotechnol. Bioeng. 91, 651–669.

Zhu, J., Winans, S.C., 2001. The quorum-sensing transcriptional regulator TraR requires its cognate signaling ligand for protein folding, protease resistance, and dimerization. Proc. Natl. Acad. Sci. U.S.A. 98, 1507–1512.

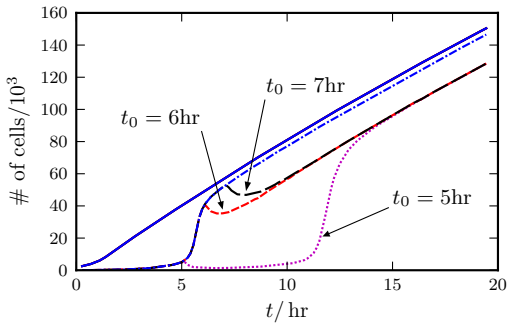

(a) $K_q = 10$, $C_{\bar{q}} = 50$

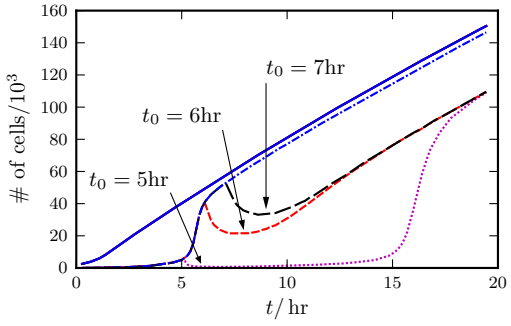

(b) $K_q = 10$, $C_{\bar{q}} = 100$

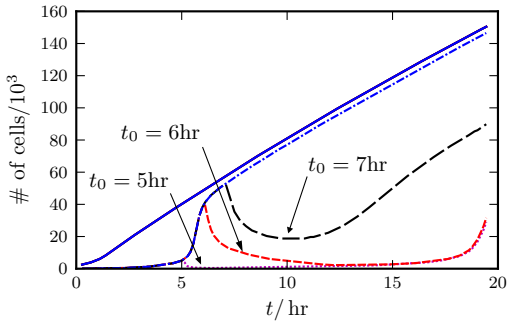

(c) $K_q = 10$, $C_{\bar{q}} = 150$

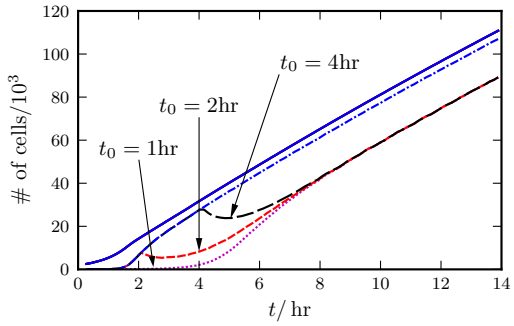

(d) $K_q = 0$, $C_{\bar{q}} = 50$

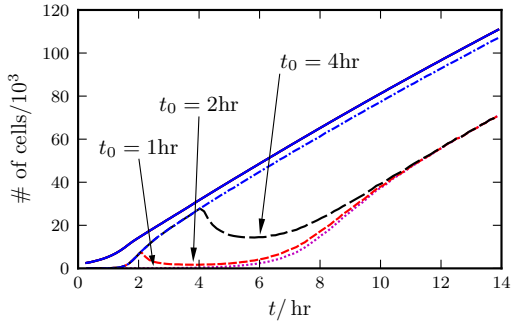

(e) $K_q = 0$, $C_{\bar{q}} = 100$

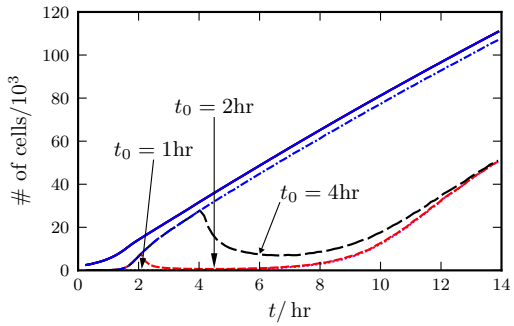

(f) $K_q = 0$, $C_{\bar{q}} = 150$

Figure 5: (colour online) Inhibition of quorum sensing in a developing biofilm. In (a)–(c), the rate of QSM production depends on its local concentration (the half-saturation constant in the QSM production rate (16) is $K_q = 10$), and the QSI concentration in the bulk compartment is set to be $C_{\bar{q}}$ at $t_0 =$ 5 hr, 6 hr, 7 hr. In (d)–(f) the QSM production rate is independent of its concentration ($K_q = 0$), and the biofilm is treated with QSI earlier ($t_0 =$ 1 hr, 2 hr, 4 hr) as up-regulation occurs earlier in these cases. The dashed and dotted lines show the number of up-regulated cells, and these diverge from that with no QSI (the dash-dotted line) at $t = t_0$.

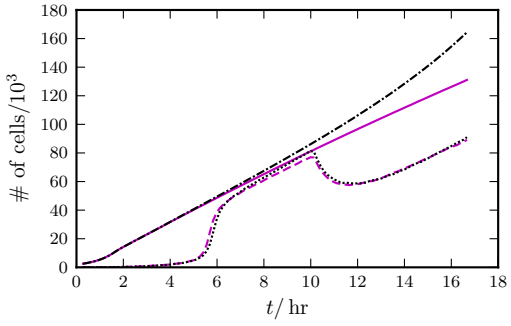

(a) $K_q = 10$

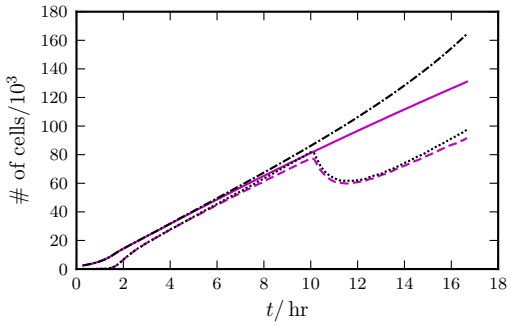

(b) $K_q = 0$

Figure 6: (colour online) Effect of EPS production on a growing biofilm. The solid and dash-dotted lines show the total numbers of cells, with low ($Z_{E,u} = 0.001$, solid magenta) and high ($Z_{E,u} = 50$, dash-dotted black) levels of EPS production by up-regulated cells, whilst the dashed (low EPS) and dotted (high EPS) lines show the corresponding numbers of up-regulated cells. At $t = 10$ hr QSI was applied (with concentration $C_{\bar{q}} = 100$ in the bulk compartment) which reduces the proportion of up-regulated cells. Here K_q is the half-saturation constant in the QSM production rate function (16).